Tribonucleation of bubbles

Sander Wildeman[a,1], Henri Lhuissier[a], Chao Sun[a], Detlef Lohse[a], and Andrea Prosperetti[a,b]

[a]Physics of Fluids Group, MESA+ Institute and J. M. Burgers Centre for Fluid Dynamics, University of Twente, 7500 AE Enschede, The Netherlands; and [b]Department of Mechanical Engineering, The Johns Hopkins University, Baltimore, MD 21218

Edited by David A. Weitz, Harvard University, Cambridge, MA, and approved May 27, 2014 (received for review November 12, 2013)

We report on the nucleation of bubbles on solids that are gently rubbed against each other in a liquid. The phenomenon is found to depend strongly on the material and roughness of the solid surfaces. For a given surface, temperature, and gas content, a trail of growing bubbles is observed if the rubbing force and velocity exceed a certain threshold. Direct observation through a transparent solid shows that each bubble in the trail results from the early coalescence of several microscopic bubbles, themselves detaching from microscopic gas pockets forming between the solids. From a detailed study of the wear tracks, with atomic force and scanning electron microscopy imaging, we conclude that these microscopic gas pockets originate from a local fracturing of the surface asperities, possibly enhanced by chemical reactions at the freshly created surfaces. Our findings will be useful either for preventing undesired bubble formation or, on the contrary, for "writing with bubbles," i.e., creating controlled patterns of microscopic bubbles.

Elementary considerations show that a bubble will spontaneously disappear unless its radius r is larger than a critical value $r_c = 2\gamma/\Delta P$, where γ is the surface tension of the liquid and ΔP is the difference between the pressure of the bubble contents and the surrounding liquid (1). Only bubbles larger than r_c can persist and grow by gas diffusion and liquid evaporation. The classical kinetic theory of nucleation (2) shows that, for water, the spontaneous formation of critical bubbles requires either superheats of 212 °C or negative pressures (i.e., tensions) of 140 MPa. Recent experiments have come close to the quantitative verification of these predictions (3, 4), but only at the cost of a great deal of sophistication and ingenuity. It must therefore be concluded that a different mechanism is responsible for the exceedingly commonplace occurrence of bubbles.

The seed for the currently accepted explanation was planted by Gernez (5) who, in 1867, hypothesized that bubbles start from a preexisting gaseous nucleus lodged in solid impurities or the walls of the container. An explanation for the stability of these heterogeneous nuclei was later supplied by Harvey et al. (6) who pointed out that the curvature induced by contact with a hydrophobic solid surface would be able to stabilize a gas pocket even in an undersaturated liquid. This "crevice model" of bubble nucleation explains a large number of observations and has been applied to the development of so-called enhanced boiling surfaces (7, 8). Gas bubbles can be further stabilized by the formation of organic skins at their surface (9, 10).

Despite these advances, the nucleation phenomenon still exhibits obscure facets, one of which—tribonucleation—is studied in this paper. It has been known for at least half a century that, as noticed by Hayward in 1967 (11), "extremely gentle rubbing" of two solid objects inside a liquid under tension, which is otherwise stable against most forms of mechanical action (e.g., knocking on the container wall or stirring), readily induces nucleation. This tribonucleation is often cited as a plausible source of the microbubbles found in the limbs of humans and animals after physical exercise (12, 13). Campbell (14) and Ikels (15) attributed the nucleation observed in these conditions to the pressure drop induced by the viscous flow in the space between two separating solid surfaces. Indeed, in highly viscous liquids, bubble formation compatible with this picture has been reported (16–18). However, this explanation cannot easily account for the nucleation observed in low-viscosity fluids like water and ethanol, because in many cases the theoretical gap between the solids would have to be smaller than the surface roughness. More strikingly, it cannot account for the key observation by Hayward that bubbles do not nucleate in the case of a rolling motion, but only in the case of a sliding motion between the solids (11), although for the same force and velocity the pressure drop is expected to be twice as large for rolling than for sliding (19). Another instance of bubble nucleation upon solid–solid contact in a low-viscosity liquid was reported by Theofanous et al. (20). These authors were able to reliably nucleate single bubbles by gently bringing into contact two stainless-steel wires in Freon superheated by up to 60 °C.

In this paper, we present experiments in which we rub a bead against a wafer submerged in a low-viscosity liquid. We vary the rubbing force and velocity, the temperature, and the materials of the solids. Our approach is to combine macroscopic observations, revealing a threshold for the rubbing-induced nucleation, with microscopic observations at the smallest scales of the problem: that of the apparent (Hertz) contact between the solids and that of the roughness tips where the actual contact is realized.

Preliminary Findings

This study was prompted by a recent observation in one of our experiments with heated liquids: bubbles are formed when the tip of a pair of stainless-steel tweezers is gently rubbed against a submerged piece of unpolished silicon wafer (Fig. 1). When the temperature of the liquid is below the boiling point, the bubbles appear as a trail behind the tweezers, where they slowly grow until they detach. After the detachment, no new bubbles are formed, indicating that the rubbing does not create permanent nucleation sites.

Significance

Microscopic gas–vapor bubbles play an important role in various processes in nature, industry, and medicine. Sometimes they are desired: to lower the temperature at which a liquid starts to boil or to enhance the contrast in medical ultrasound applications. In other cases, bubbles are harmful: they cause damage when expanding and collapsing near the propeller blades of ships, and sickness upon expanding in the veins of plants and animals. In spite of their ubiquity, the "nucleation" of bubbles, i.e., the mechanism responsible for their initial formation, has remained mysterious for a long time and, even today, it is not fully understood. Here, we show that bubbles can nucleate when two solids are gently rubbed together in a liquid: "tribonucleation."

Author contributions: S.W., H.L., and C.S. designed research; S.W. performed research; S.W., H.L., C.S., D.L., and A.P. analyzed data; and S.W., H.L., C.S., D.L., and A.P. wrote the paper.

The authors declare no conflict of interest.

This article is a PNAS Direct Submission.

[1]To whom correspondence should be addressed. E-mail: s.wildeman@utwente.nl.

This article contains supporting information online at www.pnas.org/lookup/suppl/doi:10.1073/pnas.1321194111/-/DCSupplemental.

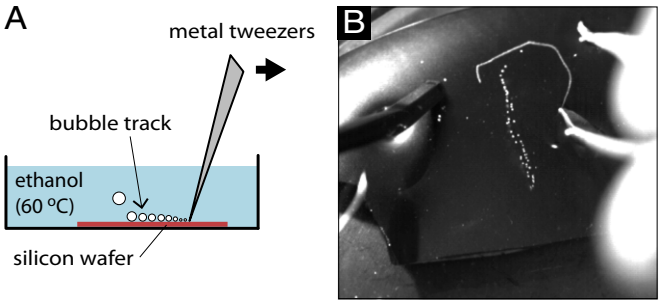

Fig. 1. (*A*) Schematic of the rubbing experiment. (*B*) Photograph of one of the authors writing a "P" with a trail of slowly growing bubbles by gently rubbing the tip of a pair of metal tweezers over a piece of unpolished silicon wafer submerged in ethanol.

This tribonucleation phenomenon occurred in all fluids we have tried so far (ethanol, water, acetone, pentane, and perfluorohexane), whether polar or not, and whether they wet the solids or not. Conversely, it depends strongly on the material of the wafer being rubbed. Bubbles appear on silicon and aluminum under mild rubbing conditions, but remain absent on copper, glass, and sapphire even upon vigorous rubbing. (Bubbles did appear at high loads on glass and sapphire with the tweezers, but not when the tweezers were replaced by a glass or sapphire bead. We think that this is because the tweezers material itself promotes the tribonucleation to some extent.)

Force–Velocity Dependence

To obtain quantitative information about the rubbing conditions for bubble formation, we used the setup sketched in Fig. 2*A*. A smooth sapphire bead (average roughness $\mathcal{R}_a < 0.025$ μm from Ceratec; radius $R = 4$ mm) attached to a movable lever arm, replaces the tweezers. A heater was placed underneath the wafer being rubbed. This allowed us to precisely control the nominal geometry of the contact, the normal force F applied to the bead, the rubbing velocity V and the temperature T of the submerged surfaces. Ethanol (99.8% from Assink Chemie; boiling point, 78 °C) was used as the liquid.

Fig. 2*B* shows a typical experiment, observed from the side through a long-distance microscope. At $t = 0$ s (*i*), the bead rubs against the unpolished side of a silicon wafer held at a temperature of 70 °C. Subsequently (*ii–vi*), small bubbles (black spots) appear behind the bead and slowly grow by gas diffusion. A theoretical estimate of the relevant timescales of this growth is provided in *SI Text*. Although ethanol wets the silicon wafer, the bubbles do not immediately detach. They are pulled down by a "Marangoni force" induced by the temperature gradient close to the wafer surface (21). Snapshots (*iii–vi*) show how two bubbles in the row merge, jump up, and then settle down again. The jumping is driven by a release of surface energy during merger, as described for droplets in ref. 22. As the bubbles grow bigger, the upward buoyancy force eventually overcomes the downward Marangoni force and they rise to the free surface (*vi*).

The experiment was repeated for different rubbing velocities and loads (Fig. 3). In each experiment, we fixed the normal force on the bead and then increased the velocity step by step, while monitoring the bubble trail behind the bead. We distinguished between a "full trail of bubbles," a "partial trail of bubbles," and "no bubbles." The data show that the higher the load, the lower the rubbing velocities required to generate bubbles. As indicated by the lines in Fig. 3, the thresholds we measured are well described by the following:

$$FV = \text{const}, \qquad [1]$$

with const = 17 and 53 μW for the lower and upper thresholds, respectively.

Influence of the Material and Surface Roughness

The fact that no sharp transition exists from no bubbles to a full trail suggests that bubble formation depends, somehow, on the varying conditions along the rubbing track. Indeed, when the polished side of the silicon wafer was rubbed, the generation of bubbles became significantly harder and less regular. Moreover, when the bead was continuously rubbed back and forth over the same track on the unpolished wafer, bubble formation stopped after typically 10–20 strokes, suggesting that rubbing locally changes the surface. If, subsequently, the bead was slightly displaced from the deactivated track during the rubbing, bubbles formed again.

Besides silicon, bubbles are also readily formed on aluminum. In Fig. 4, we compare the tribonucleation threshold for aluminum with that for silicon. To give the aluminum a macroscopic

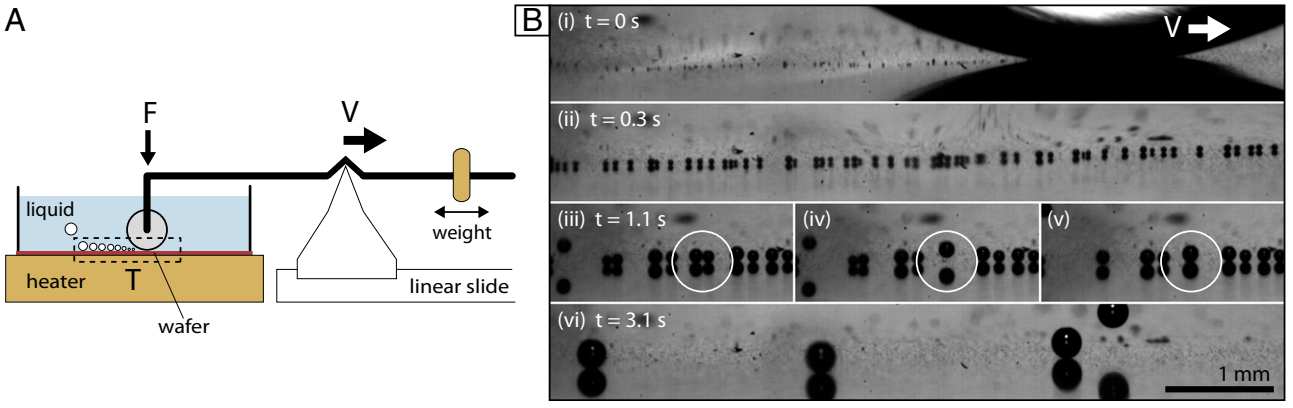

Fig. 2. (*A*) Experimental setup. It consists of a lever to control the normal force on the bead, a linear slide (connected to a linear motor) to control the rubbing velocity, and a heater to set the temperature at the bottom of the liquid cell. The wafer surface can be closely monitored from the side (dashed rectangle) or from the top with a long-distance microscope. (*B*) Side snapshots of the experiment. Due to the backlighting conditions, bubbles (and their reflection in the silicon wafer) appear as black disks against a lighter background. (*i*) A smooth sapphire bead, submerged in ethanol, is rubbed from left to right against an unpolished silicon wafer at 70 °C. (*ii*) The bubble trail left behind the bead slowly grows by gas diffusion. (*iii–v*) When two bubbles touch (see white circle), they merge, jump up, and then slowly settle down again due to the temperature gradient near the surface (Marangoni effect). (*vi*) Eventually, buoyancy overcomes the downward Marangoni force and the bubbles rise to the free surface.

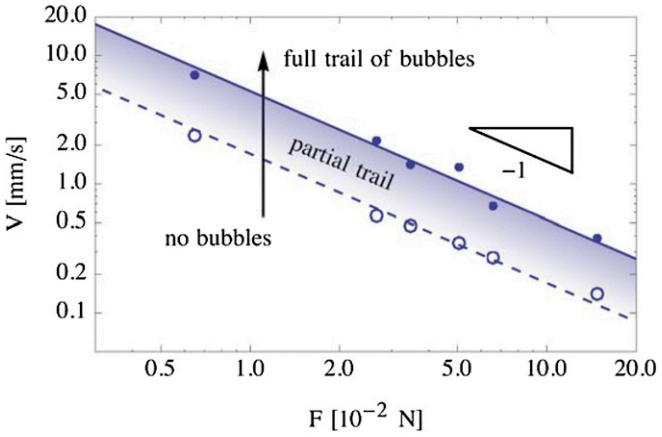

Fig. 3. Threshold velocity for the formation of a trail of bubbles as a function of the normal force, for a sapphire bead rubbing on an unpolished silicon wafer. The wafer temperature is 70 °C, and the fitted lines correspond to FV = const.

roughness similar to that of the silicon wafer ($\mathcal{R}_a \sim 0.5$ μm), the surface was sandblasted with a fine grain before the experiment. The threshold for aluminum turns out to be significantly lower than for silicon (9 μW compared with 53 μW). Moreover, in contrast to the quick deactivation of the rubbing tracks on silicon, the tracks on aluminum kept on generating bubbles even after more than 1,000 strokes (the largest value we tried), although after typically 20 strokes a polished wear track became clearly visible on the roughened aluminum. Last, when the sandblasted surface was replaced by a smooth layer of aluminum (vapor-deposited on a glass slide, $\mathcal{R}_a \sim 2$ nm), no bubbles appeared during the first rubbing stroke, but did appear in subsequent passes over the same spot, hinting that the steady-state wear track on aluminum is not smooth and promotes nucleation (as will be further discussed below).

Influence of the Temperature

In all of the experiments described so far, the temperature was kept unchanged at 70 °C (about 8 °C below the boiling point of ethanol). To determine whether and how temperature affects the generation of bubbles, we did experiments in which we ramped the temperature from 25 to 70 °C, while continuously rubbing back and forth over the same track on a polished aluminum wafer. We choose aluminum because, on it, tracks do not deactivate but keep forming bubbles as long as the force–velocity threshold is overcome, as reported above. We fixed the velocity at 2.8 mm·s^{-1} (which at 70 °C is enough to generate bubbles at very low loads) and varied the normal force between each temperature ramp. The results are shown in Fig. 5. They reveal that the lower the temperature, the higher the load required to generate a visible bubble trail. As with the force–velocity threshold (Fig. 3), there is a finite transition region from no bubbles to a full trail.

Origin of the Threshold for Bubble Trail Formation

We envision the trail formation to depend on two steps: (*i*) the inception of bubble nuclei in the contact area and (*ii*) the subsequent growth of these nuclei after the contact area has moved. To see how these steps determine the observed thresholds (Figs. 4 and 5), we set up the experiment shown in Fig. 6*A*. A piece of aluminum foil was tightly wrapped around the sapphire bead, which was then rubbed against a glass substrate submerged in ethanol. This allows for a direct observation of the contact area through the glass. To enhance the wear of the foil by the substrate, the latter was equipped with protrusions in the form of micropillars.

The direct observation of the contact area provided some crucial insights. First, as shown in Fig. 6*B*, rubbing can trigger the nucleation of bubbles on aluminum even at room temperature. During the rubbing, gas continuously comes out of solution and collects in microscopic gas pockets trapped between the two solids. As the substrate moves on, these pockets are ejected in the form of small bubbles. At room temperature, these bubbles do not grow, but dissolve as soon as they reach the bulk of the liquid. Similarly, the gas pockets trapped in the contact area slowly dissolve when the substrate motion is stopped. Second, at temperatures for which the pressure inside the bubble is large enough to make them persist, the microscopic bubbles merge, resulting in a regular trail (Fig. 2*B*). This indicates that, in Fig. 5, it is the supersaturation condition (and not the bubble inception) that dictates the trail formation.

We can quantify this idea with a model in which the size of the microscopic bubbles is set by the space available in the contact area (Fig. 7). First, we use Hertz's contact theory to estimate the radius a of the apparent contact area as follows:

$$a \sim \sqrt{\epsilon R}, \qquad [2]$$

where the indentation depth ε is related to the normal force F as follows (23):

$$\epsilon \sim \left(\frac{3}{4}\frac{F}{E^* R^{1/2}}\right)^{2/3}. \qquad [3]$$

Here E^* is the effective elastic modulus of the particular bead–substrate combination, which is dominated by the softer of the two. Combining the contact radius a with a typical roughness height h gives the volume available for all of the gas pockets as follows:

$$\Omega \sim \pi a^2 h. \qquad [4]$$

If we suppose that all this gas ends up in a single bubble of radius $r = (3\Omega/4\pi)^{1/3}$, then, as is mentioned in the introduction and elaborated on in *SI Text*, this unstable bubble will grow in the bulk if its radius is larger than the following:

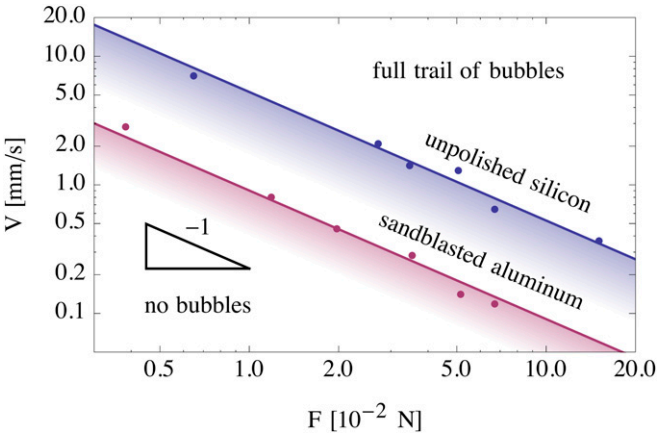

Fig. 4. Comparison between the force–velocity thresholds for unpolished silicon and sandblasted aluminum submerged in ethanol at 70 °C and having similar roughness $\mathcal{R}_a \sim 0.5$ μm. The solid lines correspond to FV = const. In the shaded area, we still observe a partial bubble trail (Fig. 3).

$$r_c = \left(\frac{3\Omega_c}{4\pi}\right)^{1/3} \sim \frac{2\gamma}{\Delta P}. \quad [5]$$

Before being heated, the liquid used in the experiments was equilibrated for a long time with air (i.e., gas plus vapor) at a temperature of $T_0 = 20$ °C; under a total pressure $P_{atm} = P_g + P_v(T_0) = 1$ bar. During the heating to a temperature T, the gas content of the liquid, i.e., $P_g \simeq P_{atm} - P_v(T_0)$, did not change appreciably (because the relevant gas diffusion timescale is much longer than that of the heating, and the gas solubility only changes by 10% over the temperature range). The excess pressure ΔP in the heated liquid therefore comes down to the increase in the vapor pressure from T_0 to T, that is, $\Delta P \simeq P_v(T) - P_v(T_0) = \Delta P_v(T)$. Combining Eqs. **2–5** yields an expression for the critical force as a function of temperature as follows:

$$F_c(T) \sim \frac{4E^*}{3R}\left(\frac{4}{3h}\right)^{3/2}\left(\frac{2\gamma}{\Delta P_v(T)}\right)^{9/2}, \quad [6]$$

with a prefactor of ~1.

Eq. **6** is plotted in Fig. 5 for $h = 50$ and 300 nm, using the surface tension $\gamma = 0.02$ N·m^{-1} of ethanol, the elastic modulus $E^* = 70$ GPa of aluminum, and an empirical relation for the ethanol vapor pressure (24). The roughness parameters of 50 and 300 nm correspond, in order of magnitude, to the large- and small-scale roughnesses we measured by atomic force microscopy (AFM) on the steady-state wear track on aluminum. The experimental data in Fig. 5 therefore seem to be consistent with our model. One crucial question, however, remains: what controls the nucleation of these gas pockets?

Microscopic Mechanism for Gas Pocket Formation

As mentioned in *Preliminary Findings*, tribonucleation is observed on aluminum, but not on copper. This prompted us to closely analyze the wear tracks left on each surface. Fig. 8 shows photographs and detailed scanning electron microscopy (SEM) recordings of wear tracks on aluminum and copper. Although the two tracks look very similar optically, they can be easily distinguished in the SEM images. Indeed, for both aluminum and copper, the asperities in the wear tracks got flattened by the rubbing bead. However, on aluminum this flattening seems to result from a continuous breaking off of small parts of the rough surface (as for a brittle material). The top surface of the flattened asperities has small scratches throughout and a lot of small wear particles are observed around, in the troughs. In contrast, for copper the top surface has a relatively low roughness, material is plastically squeezed out at the sides of the asperities, and no wear particles are observed around (as for a ductile material).

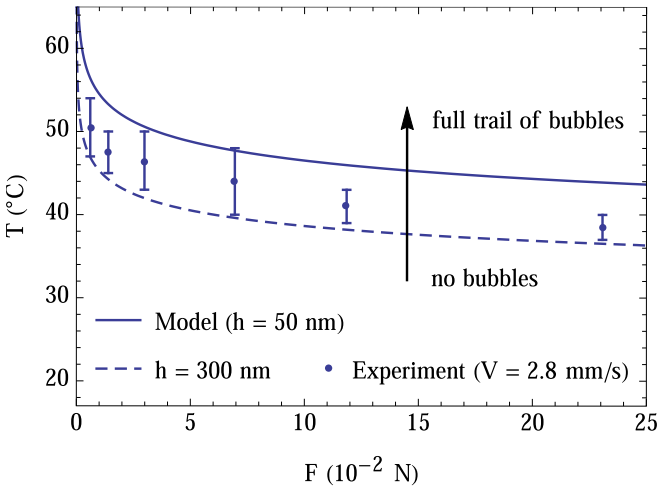

Fig. 5. Threshold temperature for bubble formation as a function of the normal force, for a smooth sapphire bead rubbed against a polished aluminum surface with velocity $V = 2.8$ mm·s^{-1}. The dots represent the experimental data, and the lines represent Eq. **6**. The single fitting parameter h can be interpreted as a measure of the typical roughness height in the wear track (see text).

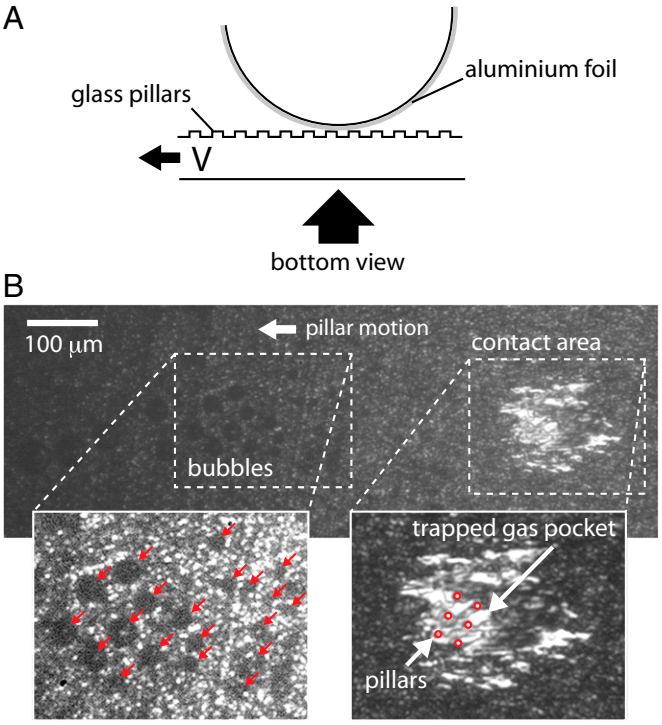

Fig. 6. (*A*) Schematic of the setup: a transparent glass surface covered with micropillars is rubbed against a bead covered with aluminum foil ($F = 7 \times 10^{-2}$ N, $V = 4.7$ mm·s^{-1}). (*B*) Bottom view of the experiment through a microscope. Gas pockets are trapped between the two solids in the contact area, and microscopic gas bubbles (red arrows) are observed downstream. The spacing between the pillars, their diameter, and their height are 10, 9, and 0.3 μm, respectively.

The comparison of the wear tracks suggests that the fracturing of the surface is an essential ingredient for a material to provoke tribonucleation. To test whether it is the fracturing itself or its products (i.e., the wear particles left on the track) that are responsible for the creation of gas pockets, we realized the experiment shown in Fig. 9. A piece of aluminum (soft Al99.5%; Salamon's Metalen) or copper (Cu99.95%; Salamon's Metalen) foil was immersed in hot ethanol and then torn apart at a constant velocity of about 9 mm·s^{-1}. Consistent with the rubbing experiments, bubbles did appear in the case of aluminum, but not in the case of copper. (Sometimes, a single bubble appeared in the very last stage, when the two ends of the copper foil completely separated at much higher velocity.) Because wear particles play no role here, this experiment shows that the fracturing itself can generate gas nuclei.

Discussion

A possible scenario for the nucleation by fracturing is that the gap formed when a microcrack opens fills with gas and vapor before the liquid can enter it. This embryo can then act as a nucleus for the formation of a visible bubble. Only in a brittle material, this crack opening would be rapid enough.

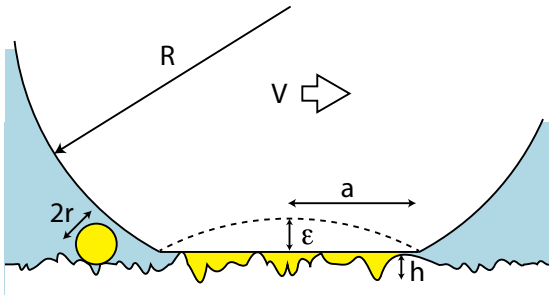

Fig. 7. Geometry used for the model. Gas (yellow) completely fills the gap in the apparent contact area and collects in a single bubble with radius *r*. For clarity, the bead is shown indented here, whereas in reality the indentation is essentially concentrated on the aluminum surface, which is much softer than the sapphire bead.

Although bulk aluminum is ductile, it has a thin (typically one nanometer thick) oxide layer on its surface, which might explain its brittle behavior. A similar layer exists on the surface of silicon. Note that this "passivation layer" forms because the bare materials readily react with any oxidizing molecules in their environment. In particular, in the presence of water, this chemical activity causes the generation of hydrogen gas, which might be at the root of, or at least contribute to, the initial nucleation process. This idea is supported by experiments with degassed water, in which we still observed the formation of microscopic gas bubbles, which quickly dissolved after the rubbing had stopped. However, we should stress that we could also create bubble trails in perfluorohexane (FC72), a liquid that should be inert in most circumstances. Also in the work by Theofanous et al. (20), which involved polished stainless steel and Freon, chemical reactions are very unlikely.

The embryos formed by the mechanism of fracturing and, possibly, chemical reactions may not grow individually, but only if they merge with others before dissolving. The force–velocity threshold FV = const. would then be a manifestation of the competition between generation, merging, and dissolution and could be interpreted as a minimal frictional power input required for abundant local fracturing.

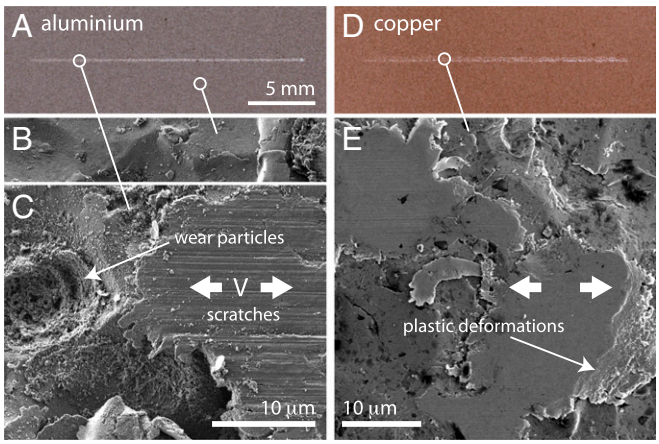

Fig. 8. Wear tracks formed by rubbing a sapphire bead 50 times back and forth against (*A*–*C*) sandblasted aluminum and (*D* and *E*) sandblasted copper. Rubbing parameters are as follows: $T = 70$ °C, $F = 7 \times 10^{-2}$ N, and $V = 1$ mm·s^{-1}. (*A* and *D*) The wear tracks are clearly visible under racking lighting and look very similar to the naked eye. (*C* and *E*) SEM imaging, however, reveals important differences at the scale of a single asperity. (*C*) On aluminum, the scratches on top of the flattened asperities are relatively deep ($\mathcal{R}_a \sim 50$ nm from AFM measurements) and many small wear particles are collected in the troughs around the asperities (as for a brittle material). (*E*) On copper, the tops of the asperities are much smoother ($\mathcal{R}_a \sim 5$ nm), they seem to be plastically squeezed, and no wear particles are observed (as for a ductile material).

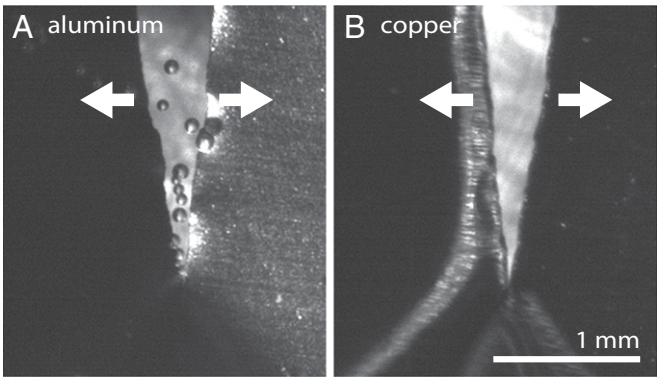

Fig. 9. Snapshots of the tearing of thin foils of (*A*) aluminum and (*B*) copper submerged in ethanol at around 78 °C. The foils are 12.0 and 12.5 μm thick, respectively, and the two sides of the foil are torn apart with a velocity of about 9 mm·s^{-1}. For aluminum, bubbles form at the tip of the tear, whereas for copper no bubbles form.

Summary and Conclusion

We have found that bubbles are readily and reliably generated upon gentle rubbing of certain solid surfaces. An intriguing demonstration of the phenomenon is the "writing" example shown in Fig. 1. It is somewhat surprising that, despite its robustness and repeatability, this phenomenon has been the object of so little attention in the literature.

We observed that bubbles can nucleate and form a trail on submerged solids under gentle rubbing conditions (normal force, F = 1–200 mN, and relative velocity, V = 0.1–20 mm·s^{-1}). At room temperature, small bubbles are observed to form and detach, but they dissolve as they move away from the contact area. As the temperature is increased, the bubbles persist and grow, forming a trail. On silicon and aluminum, measurements in ethanol at 70 °C and above indicate the existence of a threshold for the trail formation of the form FV = const., with a constant six times larger for silicon than for aluminum.

Bubble formation strongly depends on the materials being rubbed. On silicon, tribonucleation stops after typically 20 strokes over the same spot, whereas on aluminum a steady-state wear track forms from which bubbles keep appearing upon rubbing. Bubbles do not form on copper, although the wear tracks on copper and aluminum look very similar optically. SEM imaging shows that aluminum asperities are abraded by a fracturing, brittle-like mechanism, whereas copper asperities are flattened by plastic, ductile-like deformations. Additional experiments on the slow rupture of aluminum and copper foils indicate that fracturing alone (in the absence of wear) is sufficient to create gas nuclei.

The above observations evidence that trail formation by tribonucleation involves two steps: (*i*) bubble nucleation in the contact region and (*ii*) subsequent growth of these nuclei in the bulk. Both steps need to be satisfied to see a trail. Our experiments show that fracturing is essential for the first step. We hypothesize that a void created by the rapid fracturing of the surface asperities, possibly in combination with chemical reactions forming gas at the freshly created surfaces, can explain the nucleation of bubbles at the low loads and velocities used in the experiments. When there is abundant local fracturing, the amount of gas that comes out of solution is limited by the space

available between the asperities of the surfaces in contact, and it is this volume that sets the threshold for trail formation in this case.

We hope that the present exploratory work may motivate further studies to look into the fundamental mechanism(s) involved in tribonucleation, and to explain, for example, the emergent dependence of the phenomenon on the rubbing force and velocity.

ACKNOWLEDGMENTS. We thank Yanbo Xie for providing us with structured glass substrates, Gert-Wim Bruggert for his assistance with the design and implementation of the setup, Robin Berkelaar for help with scanning the wear tracks with an AFM and interpreting the images, Mark Smithers and Gerard Kip, associated with the MESA+ Institute, for making high-resolution SEM recordings for us, Erik de Vries from the Surface Technology and Tribology Group for useful discussion on the wear track images, Vincent Craig for emphasizing the possible role of chemistry in the experiments, and an anonymous referee for useful suggestions. This project was financed by a European Research Council Advanced Grant.

1. Brennen CE (1995) *Cavitation and Bubble Dynamics* (Oxford Univ Press, Oxford).
2. Skripov V (1974) *Metastable Liquids* (Wiley, New York).
3. El Mekki Azouzi M, Ramboz C, Lenain J-F, Caupin F (2013) A coherent picture of water at extreme negative pressure. *Nat Phys* 9(1):38–41.
4. Zheng Q, Durben DJ, Wolf GH, Angell CA (1991) Liquids at large negative pressures: Water at the homogeneous nucleation limit. *Science* 254(5033):829–832.
5. Gernez M (1867) On the disengagement of gases from their saturated solutions. *Philos Mag* 33(225):479–481.
6. Harvey EN, et al. (1944) Bubble formation in animals. I. Physical factors. *J Cell Comp Physiol* 24(1):1–22.
7. Kotthoff S, Gorenflo D, Danger E, Luke A (2006) Heat transfer and bubble formation in pool boiling: Effect of basic surface modifications for heat transfer enhancement. *Int J Therm Sci* 45(3):217–236.
8. Webb R (2005) Odyssey of the enhanced boiling surface. *J Heat Trans* 126(6):1051–1059.
9. Fox FE, Herzfeld KF (1954) Gas bubbles with organic skin as cavitation nuclei. *J Acoust Soc Am* 26(6):984–989.
10. Yount DE (1979) Skins of varying permeability: A stabilization mechanism for gas cavitation nuclei. *J Acoust Soc Am* 65(6):1429–1439.
11. Hayward ATJ (1967) Tribonucleation of bubbles. *Br J Appl Phys* 18:641–644.
12. McDonough PM, Hemmingsen EA (1984) Bubble formation in crabs induced by limb motions after decompression. *J Appl Physiol* 57(1):117–122.
13. Wilbur JC, et al. (2010) Signals consistent with microbubbles detected in legs of normal human subjects after exercise. *J Appl Physiol (1985)* 108(2):240–244.
14. Campbell J (1968) The tribonucleation of bubbles. *Br J Appl Phys* 1(8):1085–1088.
15. Ikels KG (1970) Production of gas bubbles in fluids by tribonucleation. *J Appl Physiol* 28(4):524–527.
16. Ashmore J, del Pino C, Mullin T (2005) Cavitation in a lubrication flow between a moving sphere and a boundary. *Phys Rev Lett* 94(12):124501.
17. Prokunin AN (2004) Microcavitation in the slow motion of a solid spherical particle along a wall in a fluid. *Fluid Dyn* 39(5):771–778.
18. Chen YL, Israelachvili J (1991) New mechanism of cavitation damage. *Science* 252(5009):1157–1160.
19. O'Neill ME, Stewartson K (1967) On the slow motion of a sphere parallel to a nearby plane wall. *J Fluid Mech* 27(4):705–724.
20. Theofanous TG, Bohrer TH, Chang MC, Patel PD (1978) Experiments and universal growth relations for vapor bubbles with microlayers. *J Heat Trans* 100(1): 41–48.
21. Young NO, Goldstein J, Block MJ (1959) The motion of bubbles in a vertical temperature gradient. *J Fluid Mech* 6(3):350–356.
22. Boreyko JB, Chen CH (2009) Self-propelled dropwise condensate on superhydrophobic surfaces. *Phys Rev Lett* 103(18):184501.
23. Landau L, Lifshitz E (1970) *Theory of Elasticity* (Pergamon, Oxford), 2nd Ed.
24. Ambrose D, Sprake CHS (1970) Thermodynamic properties of organic oxygen compounds xxv. vapour pressures and normal boiling temperatures of aliphatic alcohols. *J Chem Thermodyn* 2(5):631–645.

Supporting Information

Wildeman et al. 10.1073/pnas.1321194111

SI Text

Timescale of Diffusive Bubble Growth in a Hot Liquid. In the experiments described in the paper, a liquid saturated with dissolved air at room temperature T_0 is heated to a higher temperature T below its boiling point T_B. The growth of bubbles nucleated in this hot liquid hinges on the fact that the equilibrium condition $r = r_c$, with $r_c = 2\gamma/\Delta P$, is unstable when the amount of gas and vapor in the bubble is not constrained to be constant. Here, we provide a more detailed description of how this instability leads to the bubble growth that we observe.

For $T < T_B$, the growth process is sufficiently slow so that inertia can be neglected, as in the classic paper by Epstein and Plesset (1) on the diffusive growth of gas bubbles. We also assume for now that surface tension can be neglected, which will be justified below. With these assumptions, the sum $P_g + P_v$ of the gas and vapor partial pressures in a bubble (however nucleated) will essentially be equal to the ambient atmospheric pressure P_{atm} at all times.

Before raising the temperature, the liquid had been in contact with the surroundings long enough to ensure that it was uniformly saturated with dissolved air at the initial room temperature T_0. According to Henry's law, this initial dissolved gas concentration would have been $C^{(0)} = P_g^{(0)}/k(T_0) = [P_{atm} - P_v(T_0)]/k(T_0)$, in which k is the temperature-dependent Henry's constant. Once a bubble is nucleated in the hot liquid, the constraint $P_g + P_v = P_{atm}$, together with the fact that $P_v(T) > P_v(T_0)$, implies that the gas partial pressure inside it will be lower than $P_g^{(0)}$. As a consequence, again by Henry's law, the dissolved gas concentration at the bubble surface would take a value $C^{(i)} = [P_{atm} - P_v(T)]/k(T) < C^{(0)}$ while, in view of the slowness of the mass diffusion process (compared with the heating rate), the bulk concentration in the liquid (i.e., far from the bubble surface) remains at the initial value $C^{(0)}$. This circumstance sets up a concentration difference between the bubble surface and the bulk liquid given by the following:

$$\Delta C = C^{(0)} - C^{(i)} = \frac{P_{atm} - P_v(T_0)}{k(T_0)} - \frac{P_{atm} - P_v(T)}{k(T)} \approx \frac{\Delta P_v}{k}, \qquad \textbf{[S1]}$$

where $\Delta P_v = P_v(T) - P_v(T_0)$, and, in the last step, we have neglected the small temperature dependence of the Henry's constant, which is inconsequential in the temperature range of present concern.

According to ref. 1, the radius r of a bubble in a gas-supersaturated liquid grows at the following approximate rate:

$$\dot{r} = \frac{D\Delta C}{\rho_g}\left(\frac{1}{r} + \frac{1}{\sqrt{\pi D t}}\right), \qquad \textbf{[S2]}$$

where ρ_g is the density of the gas in the bubble, D is the gas diffusivity in the liquid, t is time, and concentration is expressed in kilograms per cubic meter. The asymptotic solution of this equation, valid for radii much larger than the initial value, takes the following form (1):

$$r^2 = 2\left[\lambda + \sqrt{1+\lambda^2}\right]^2 \frac{D\Delta C}{\rho_g} t, \qquad \textbf{[S3]}$$

with $\lambda \equiv \sqrt{\Delta C/(2\pi\rho_g)}$.

For air in ethanol at $T = 70$ °C, we have $k = 3 \times 10^5$ m^2/s^2 (an order of magnitude smaller than for water), $\rho_g = 0.3$ kg/m^3, $D = 10^{-8}$ m^2/s, and $\Delta P_v = 70$ kPa. Making use of these values and of Eqs. **S1** and **S3**, we find that a bubble grows to the typical detachment radius $r = 0.15$ mm observed in the experiments in ∼0.8 s. This duration corresponds in order of magnitude to the growth time observed in the experiments (∼3 s; Fig. 2 of the main text), but it represents an underestimation of the actual growth time as it neglects the hindrance to diffusion caused by the solid surface and the competition for dissolved gas due to the growth of the neighboring bubbles. The real situation is further complicated by the merging and jumping of the bubbles.

Last, we can estimate the influence of surface tension, which we neglected above. Surface tension is important close to the nucleation threshold $r_c = 2\gamma/\Delta P_v$, and we thus consider a bubble with radius $r = (1 + \varepsilon)r_c$, where $\varepsilon \ll 1$ is a small parameter. The bubble grows only if $\varepsilon > 0$, because in this case the gas partial pressure inside the bubble, which balances the external atmospheric pressure, is smaller than that required for thermodynamic equilibrium by the following:

$$\Delta P_\gamma = 2\gamma\left(\frac{1}{r_c} - \frac{1}{r}\right) \simeq \frac{2\gamma}{r_c}\epsilon = \Delta P_v \epsilon. \qquad \textbf{[S4]}$$

Gas diffusion is also the limiting mechanism here. We thus make use of Eq. **S2** with the effective concentration difference $\Delta C_\gamma = \Delta P_\gamma/k = 2\gamma\varepsilon/r_c k$, and taking into account the compressibility of the gas via the effective gas density $\rho_g^* = \rho_g + 4\gamma/3R_g T r_c = 0.7$ kg/m^3 (1), where $R_g = 290$ J/kg·K is the specific gas constant of the gas, to find the following:

$$\dot{\epsilon} = \frac{2D\gamma}{\rho_g^* r_c^2 k}\left(\frac{1}{r_c} + \frac{1}{\sqrt{\pi D t}}\right)\epsilon. \qquad \textbf{[S5]}$$

This yields the following exponential growth:

$$\epsilon(t) = \epsilon_0 \exp\left(\frac{t}{\tau_1} + \sqrt{\frac{t}{\tau_2}}\right), \qquad \textbf{[S6]}$$

in which the timescales are $\tau_1 = \rho_g^* k r_c^3/2D\gamma$ and $\tau_2 = \pi\rho_g^{*2} k^2 r_c^4/16D\gamma^2$. With $\gamma = 18$ mN at $T = 70$ °C, this gives $\tau_1 \simeq 0.1$ ms and $\tau_2 \simeq 0.3$ ms, which means that the delay induced by surface tension on the growth time derived from Eq. **S3** is indeed negligible.

1. Epstein PS, Plesset MS (1950) On the stability of gas bubbles in liquid-gas solutions. *J Chem Phys* 18(11):1505–1509.